Acta Astronautica 208 (2023) 381–388

Contents lists available at ScienceDirect

Acta Astronautica

journal homepage: www.elsevier.com/locate/actaastro

Research paper

Cross-verification and benchmarking analysis of electrodynamic tether simulators

Gabriel Borderes-Motta [a,b,*], Gabriel de Haro-Pizarroso [a], Gangqiang Li [c], Hanze Yu [c], Zheng H. Zhu [c], Giulia Sarego [d], Giacomo Colombatti [d], Enrico C. Lorenzini [d], Jesse K. McTernan [e], Brian E. Gilchrist [f], Sven G. Bilén [e], Satomi Kawamoto [g], Yasushi Ohkawa [g], Gonzalo Sánchez-Arriaga [a]

[a] Universidad Carlos III de Madrid (UC3M), Spain
[b] Swedish Institute of Space Physics (IRF), Sweden
[c] York University (YU), Canada
[d] Universitá degli Studi di Padova (UNIPD), Italy
[e] The Pennsylvania State University (PSU), USA
[f] University of Michigan (U-M), USA
[g] Japan Aerospace Exploration Agency (JAXA), Japan

ARTICLE INFO

Keywords:
Electrodynamic tethers
Mission analysis
Space debris

ABSTRACT

Five electrodynamic tether simulators (BETsMA v2.0, DYNATETHER, EDTSim, FLEX, and TeMPEST) have been cross-verified by running and analysing simulations of increasing complexity. A set of ten simulations without any tether was run to test the orbital propagators and the implementation of the perturbation force due to the non-sphericity of the Earth and its non-homogeneous mass distribution. The environmental models of the five codes and their implementation were then cross-verified by analysing the evolution of the magnetic field and the plasma and atmospheric densities. The electric modules of the simulators for electrodynamic tethers working in the passive mode, i.e., the routines in charge of computing the current and the voltage profiles along the tethers as well as the Lorentz force, were compared by running simulations with bare tethers. Configurations with an ideal electron emitter (zero potential drop), a real emitter, and a resistor and an ideal emitter were considered, as well as round and tape tethers. The electric models of BETsMA, EDTSim, FLEX, and TeMPEST, which assumed a straight tether, were also compared with the result of DYNATETHER for curved tethers. The consistency of the five simulators as a whole was tested by preparing performance maps with the deorbit time versus orbit inclination for a reference scenario and considering tape and round electrodynamic tethers. Although they implement different models and make different assumptions, the results of the five codes are consistent for the full simulation campaign. The simulation data and the software to visualize them are available in a public repository.

1. Introduction

Electrodynamic tethers (EDTs) were introduced more than half a century ago [1] as a promising technology for providing in-orbit propulsion without using propellant [2]. More than 15 experiments have been flown in orbit to test EDTs, with the Plasma Motor Generator (PMG) EDT experiment being the first to demonstrate the operation of an EDT in both the active and passive modes [3]. In parallel to hardware development, numerical simulators rapidly became an effective tool to study, understand, and assess a plethora of interesting phenomena inherent to EDTs. They cover a broad range of aspects, limited not only to mission analysis, such as tether dynamics and control, risk assessment, and performance determination, but also to relevant scientific subjects such as EDT–plasma current exchange. For instance, particle-in-cell simulations [4–10] and stationary [11–13] and non-stationary [14] Eulerian solvers enabled the study of current collection to and emission from EDT systems. With respect to simulation tools aimed at mission analysis and performance determination, research groups, space agencies, and companies have developed a number of software packages for EDT system assessment, such as TetherSim^{TM} [15], TeMPEST [16], FLEX [17],

* Corresponding author at: Universidad Carlos III de Madrid (UC3M), Spain.
E-mail address: gabriel.borderes.motta@irf.se (G. Borderes-Motta).

https://doi.org/10.1016/j.actaastro.2023.04.015
Received 2 December 2022; Received in revised form 25 February 2023; Accepted 5 April 2023
Available online 8 April 2023

DYNATETHER (DYNAT) [18], BETsMA [19,20], and EDTSim [21], among many others [22–30].

As explained in several monographs [31–34], one of the challenges in EDT simulation lies in handling the disparate frequencies that naturally appear in tether dynamics, including the slow in-plane and out-of-plane oscillations, the moderate lateral string modes, and the fast longitudinal modes. Accordingly, several types of tether models of different fidelity and computational cost have been developed. For instance, the simplest model just propagates the orbit of the satellite and incorporates the action of the Lorentz force by assuming a certain attitude for the tether. Two examples are the tether being aligned with the local vertical or spinning at a certain rate inside the orbital plane. The one-bar tether model captures in-plane and out-of plane dynamics, whereas N-bar tether models incorporate tether flexibility effects. Tether elasticity introduces high frequencies and are simulated by lumped mass and continuous models. Direct application of Newton's Second Law, Lagrangian and Hamiltonian methods, Kane's Equation, and Minakov theory [35] have been used to write the equations of motion (find an excellent review in Ref. [36]).

EDT simulators are complex numerical tools that include one or more environment modules and electric and dynamic models for the tether. Additionally, and depending on the degree of fidelity and completeness of the simulator, a tether thermal model and a risk module to compute the collision probability and the tether cut probability by small debris may also be included. The most common approach for verifying the simulators is testing each module independently and analysing certain canonical solutions for which analytical predictions exist. For instance, the electric model of the tether can be compared with specialized work on that topic [37–39] and small tether oscillations around the local vertical should be consistent with linear theory. Nonetheless, an holistic comparison and the preparation of reference scenarios, which would both contribute considerably to progress in the field, are not available. The purpose of this work is to fill this gap and share with the tether community a database of simulations, metafiles, and visualization software that will allow cross-verification of any EDT simulator.

To achieve this goal, this work presents a cross-verification and benchmarking analysis of five EDT tether simulators developed by independent research groups. These simulators are

- BETsMA: Bare Electrodynamic Tether Mission Analysis. Universidad Carlos III de Madrid.
- DYNATETHER (DYNAT); Dynamic Space Tether Simulator. York University.
- EDTSim; ElectroDynamic Tether Simulator. Japan Aerospace Exploration Agency.
- FLEX; FLEXible tether dynamics simulator. University of Padova.
- TeMPEST: TEthered Mission Planning and Evaluation Software Tool. University of Michigan and Pennsylvania State University.

After verifying the simulators' orbit propagators and gravitational perturbation force, their environmental models in charge of computing the magnetic field and the plasma and neutral densities were evaluated. Following this stepwise approach, it then presents results on the testing of the tether electrodynamic models by considering a point-like approach for the satellite–tether system. Finally, it presents a parametric analysis varying the orbit inclination of the tether performance in a practical scenario: the deorbiting of space debris. The simulation results, and software to read and visualize the data, are public and available at the repository [40]. Such a source of information may be useful for new code developers and tether system developers who wish to cross-verify their own EDT simulators.

2. General considerations

In order to simplify the cross-verification of other simulators with the results of this work, the analysis starts with the simplest configuration in Section 3 and increases the complexity progressively in Sections 4 and 5. Tables with a code number for each simulation are provided in Appendix. For instance, simulation OPE1 corresponds with the first simulation aimed at the verification of the Orbit Propagators and the Environmental models. For each simulation, there is a folder named with the corresponding code in the public repository [40] that contains the results of the EDT simulators and a simple code to read and plot them. Since the five numerical tools considered in this work have different capabilities, computational cost, and implemented models, there are some simulations that were not run for certain simulators. For these cases, the folder contains only the results for a subset of the five simulators considered in this work.

Table 1
Common parameters used in the analysis.

Parameter	Value	Parameter	Value
R_e	6378.136303 km	μ_e	3.98600×10^{14} m^3/s^2
β_s	45.5 kg/m^2	C_D	2
w_t	2 cm	h_t	50 μm
L_t	2 km	R_t	2 mm
σ_t	3.54×10^7 1/Ωm	ρ_t	2700 kg/m^2
M_s	500 kg		

Table 1 summarizes the values of the parameters that are fixed for all of the simulations. For instance, when aerodynamic drag is included in the simulation, C_D is the drag coefficient of the satellite and M_s/β_s is the cross-sectional area of the satellite, where M_s is the total system mass (satellite and tether). For simulations with tape-like tethers, the length, width, and thickness are $L_t \times w_t \times h_t$ and, for round tethers, the length and radius are $L_t \times R_t$. Tether density and conductivity are ρ_t and σ_t, respectively. The Earth radius and gravitational parameter are R_E and μ_E, respectively.

Each of the five EDT simulators considered in this work implements a different set of physical models and numerical algorithms. Consequently, a perfect match among their results would not be expected. For the same reason, we do not compare the simulation results by plotting the difference of the output variables; rather, we decided to present the variables versus time. The goal of this work is not to look for a match between the simulators that does not exist because they are implemented differently, neither is it to adapt or combine the simulators to construct one with the best performances and fidelity. The objective of the study is to cross-verify the software, understand and critically discuss the results, demonstrate their consistency, and share the data to open the possibility of cross-verifying other EDT simulators. The data and the software to plot and analyse them are both public [40] and available for further research based on that presented in this work.

3. Orbit propagators and environmental models

As shown in Table 2, BETsMA, EDTSym, and TeMPEST use special orbit propagators like DROMO [41], Gauss, and Cowell, and DYNAT and FLEX directly integrate Newton's Second Law in the form $\boldsymbol{F} = m\boldsymbol{a}$ for the satellites and the particles that are used to discretize the tether. The five simulators, except TeMPEST, incorporate high harmonics of Earth's gravitational perturbations up to different orders. Although not explicitly shown in the table, the perturbations due to the electrodynamic force on the tether and the aerodynamic drag acting on the satellite and the tether can be turned on/off according to the needs of the analysis.

Table A.1 summarizes the 10 simulations with different initial orbital elements and gravitational perturbations that have been selected to verify the Orbit Propagators and the Environmental (OPE) models. In these simulations, we did not consider any tether or, if the use of a tether is mandatory in the numerical tool due to its architecture, a negligible tether length without Lorentz force and atmospheric drag was used. Therefore, we basically propagated the orbit of the satellite under the action of the gravity field. In OPE 1 and OPE 2 we verified that, without any perturbation, BETsMA and TeMPEST provide the

Table 2
Basic properties of EDT simulators. Numerical integrators are Runge–Kutta (RK), Runge–Kutta–Fehlberg (RKF), Gauss–Legendre (GL), and Radau (R). Gravitational perturbations are Spherical Harmonics (SH) of the Earth's gravitational field with the maximum order available in the model inside brackets.

Simulator	Orbit propagator	Numerical integrator	Gravitational perturbation
BETsMA	DROMO [41]	RK, RKF, R	SH (4th)
DYNAT	Not Required	RK, RKF, GL	SH (13th)
EDTSim	Gauss	RK	SH (70th)
FLEX	Cowell	RKF, R	SH (4th)
TeMPEST	Cowell	RK	N/A

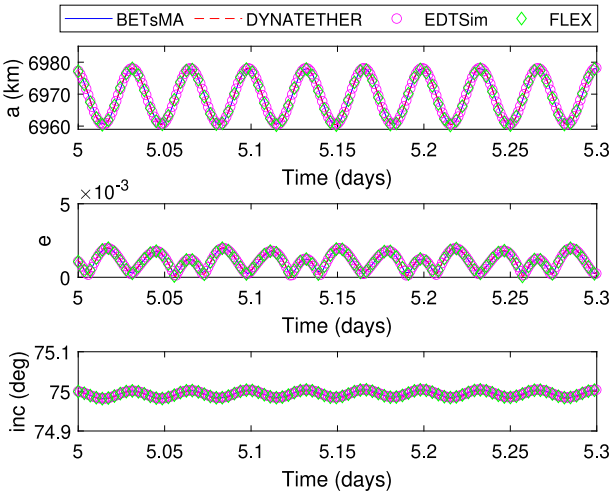

Fig. 1. Evolution of the orbital elements in simulation OPE 9.

Keplerian orbit. Simulations OPE 3 to 8 show that BETsMA, DYNAT, and FLEX give the same orbit under the J_2 perturbation for different eccentricities and inclinations. Finally, in OPE 9 and 10, we compared the result of these three simulators with EDTSym when Earth's harmonics up to order 4 are included. As an example, we show in Fig. 1 the evolution of the semimajor axis, the inclination, and the eccentricity at the fifth day of simulation with label OPE 9 for BETsMA, DYNAT, FLEX, and EDTSim. According to simulations OPE 1–10, the orbit propagators, numerical integrators, and the gravitational perturbations, are consistent among the five simulators.

Since the orbits in simulations OPE 1–10 are the same for the five tools, this set of simulations can be also used to benchmark the environmental models. As shown in Table 3, the codes handle Earth's magnetic field model of disparate complexity, several versions of the International Reference Ionosphere (IRI) model to compute the plasma density, and different models for the atmospheric density. BETsMA also has an integrated database of the debris flux obtained from MASTER 2009 and ORDEM 2000 to compute the tether cut probability by small debris during the simulation. In the case of EDTSim, the software is compatible with a separate code that uses MASTER8 and ORDEM 3.1 to assess the mission risk.

Fig. 2 shows the evolution of the three components of the magnetic field in the Geocentric Equatorial Inertial frame given by the International Geomagnetic Reference Field (IGRF) model for BETsMA, DYNAT, EDTSim, and FLEX in simulation OPE 9. The match among these four numerical tools is good. The same study and conclusion was found for OPE 1 and OPE 2 by comparing BETsMA and TeMPEST. As a related product of this analysis we also compared the component along the local vertical of the motional electric field, i.e., $E_m = (\boldsymbol{v}_{rel} \times \boldsymbol{B}) \cdot \boldsymbol{r}/r$, which involves the magnetic field and the relative velocity between the spacecraft and the ambient plasma $\boldsymbol{v}_{rel}$. This is a key variable for EDTs because it appears naturally in the electric module (see Section 4). A good match was found in OPE 1–10 for the five simulators.

Table 3
Environmental Models. Magnetic field models: Dipole (D) and Eccentric Dipole (ED).

Simulator	Magnetic field	Plasma properties	Atmospheric density	Debris flux
BETsMA	D, ED IGRF 2005	IRI 2012	NRLMSISE-00 CIRA	MASTER 2009 ORDEM 2000
DYNAT	D, ED IGRF 2020	IRI 2012	NRLMSISE-00	–
EDTSim	D, ED IGRF 2012	IRI 2016	NRLMSISE-00	MASTER 8 ORDEM 3.1
FLEX	D, ED IGRF 2005	IRI 2012	NRLMSISE-00	–
TeMPEST	IGRF 1991	IRI 1990	MSIS-86 CIRA	–

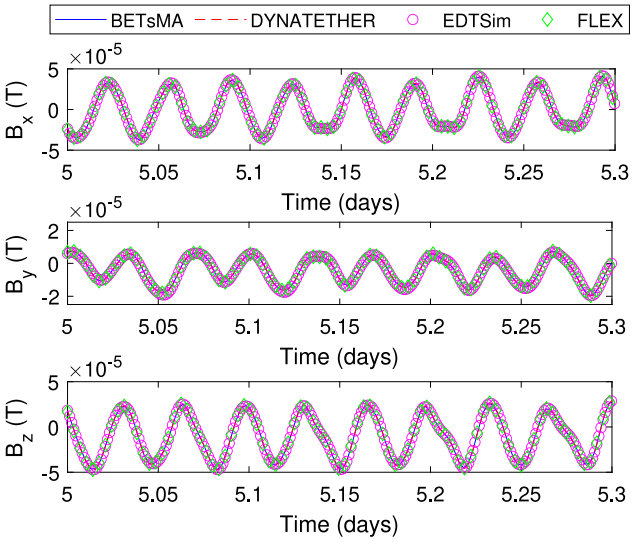

Fig. 2. Evolution of the magnetic field components in the Geocentric Equatorial Inertial frame in simulation OPE 9.

The cross-verification of the plasma density is a bit more complex because, although the five numerical tools use the International Reference Ionosphere (IRI), each simulator implements a different version. Even if two simulators were to use the same version, the outputs provided by the codes could be different due to a different configuration of their input parameters and data file. Nonetheless, the plasma densities obtained from BETsMA, EDTSim, and FLEX in OPE 9 (see top panel in Fig. 3) present a very good match. The same conclusion was found for the atmospheric density (see bottom panel in Fig. 3). Some differences were observed for DYNAT. The comparison of BETsMA and TeMPEST in OPE 1 and 2 (not shown) reveals that the profiles versus time present the same features (for instance the variations in day and night-side conditions), but the plasma density and the atmospheric density from TeMPEST is up to a 30% larger. As shown in Section 5, such a difference translates to a deviation in the assessment of tether performances.

4. Tether electrical models

The electrical models are one of the most integral elements of EDT simulators. Since they are responsible for computing the current and voltage profiles throughout the tether, they are essential for evaluating the Lorentz perturbation. As shown in Table 4, the five simulators consider a bare EDT equipped with an active Electron Emitter (EE). They primarily use the high-bias orbital-motion-limited (OML) law for electron collection [37] and an EE model that considers the emission of any current at a cost of a potential drop $V_C < 0$. In the case of BETsMA, the code also includes low-work-function tether [36,42] and bare-photovoltaic tether models [43]. In general, tethers can be

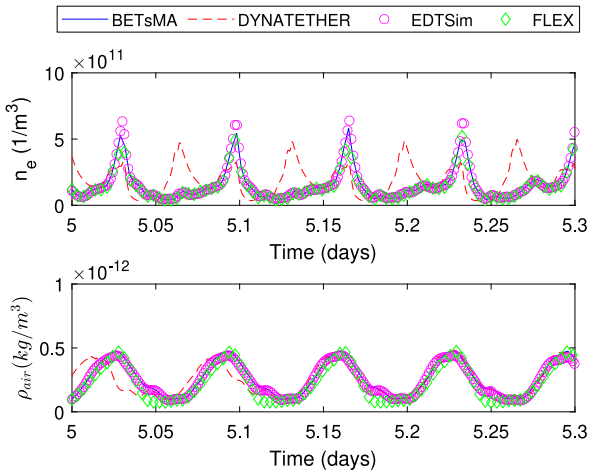

Fig. 3. Evolution of the plasma density (top) and air density (bottom) in simulation OPE 9.

Table 4
Electric Models. EDT Type: Bare tether equipped with active Electron Emitter (Bare+EE) and Low-Work-Function Tether (LWT). Operation modes: Active (A) and Passive (P). Operation submodes: Standard (S), Current Limited (CL), Current Constant (CC), Power Harvesting (PH), Constant Power (CP), Station-Keeping (SK), Libration Suppression (LS). Tether attitude model: Aligned with the local Vertical (ALV), Spinning inside the orbital plane at a constant rate (S), Self-consistently (SC) found by solving a tether dynamic model that can be an N-bar model, a lumped mass model (LM), or a continuous tether model (CM).

Simulator	EDT type	Cross section	Mode (Submodes)	Tether attitude
BETsMA	Bare+EE LWT BPT	Tape Round	P (S, CL, PH, CC, CP) A (CP, CC, SK)	ALV, S, SC (N-bar, LM)
DYNAT	Bare+EE	Tape	P (S, CL, PH) A (CP, CC, SK)	ALV, S SC (CM)
EDTSim	Bare+EE	Tape Round	P (S, CL, PH, LS) A (CP, CC, SK)	SC (LM)
FLEX	Bare+EE	Tape	P (S, CL, PH)	ALV, SC (LM)
TeMPEST	Bare+EE	Round	P (S, PH) A (CP)	ALV

operated in the passive mode ($E_m = (\boldsymbol{v}_{rel} \times \boldsymbol{B}) \cdot \boldsymbol{u}_t > 0$) and in the active mode ($E_m = (\boldsymbol{v}_{rel} \times \boldsymbol{B}) \cdot \boldsymbol{u}_t < 0$), where $\boldsymbol{u}_t$ is an unit vector pointing from the EE to the opposite tether tip.

4.1. The passive mode

The standard configuration of an EDT in the passive mode ($E_m > 0$) is a bare tether connected to the EE. In low Earth orbit (LEO), it produces a drag force that deorbits the spacecraft. If a variable resistor of electrical resistance R is located between them, the electric current can be limited and power can be harvested. If the resistor is substituted by a power source that injects a power W_e, the electric current and the EDT performance are enhanced [20]. Making the current flow through the resistor or the power supply, and selecting appropriate instantaneous values for $R(t)$ and $W_e(t)$, enable the possibility of keeping the electric current constant at the EE. An adequate control law for the variable resistor can be also used to suppress the libration of EDTs. Regarding a tether in the active mode, which produces a thrust force in LEO, the system can be operated with constant power or with non-constant power to keep the current at the EE constant or to facilitate station keeping. Although we did not cross-verify all of these tether modes and submodes in this work, Table 4 presents a summary of the software capabilities in terms of operation modes and physical models for the anodic and the cathodic contacts.

To test the electrical models, we considered the initial conditions and time given in the caption of Table A.2 and the parameters of Table 1. This set of simulations includes the Lorentz perturbation and we considered tape-like and round tethers depending on the capabilities of the software (see Table 4). Simulations with BETsMA, FLEX, and TeMPEST kept the tether attitude constrained along the local vertical, whereas DYNAT and EDTSym also simulated the dynamics of the tether attitude. Consequently, the trajectory provided by each software was different. However, as explained below, this is irrelevant for the effective comparison of the electrical model when appropriate dimensionless variables are used.

The normalized average current,

$$i_{av} \equiv \frac{1}{E_m \sigma_t A_t} \frac{1}{L} \int_0^L I(x) dx, \tag{1}$$

depends on the following dimensionless parameters for a straight tether operating in the passive mode [20,37]

$$i_{av}^P \left(\xi_t \equiv \frac{L_b}{L_*}, \phi_C \equiv \frac{V_C}{E_m L_*}, \frac{R \sigma_t A_t}{L_*}, \frac{W_e}{E_m^2 \sigma_t A_t L_*} \right), \tag{2}$$

where L_b is the length of the bare tether and L_* is the characteristic length that gauges ohmic effects: [37]

$$L_* \equiv \left(\frac{2A_t}{p_t} \right)^{2/3} \left(\frac{9\pi^2 m_e \sigma_t^2 |E_m|}{128 e^3 N_0^2} \right)^{1/3}. \tag{3}$$

Ignoring ion collection, and for $V_C = W_e = R = 0$, the normalized average current takes the form [44]

$$i_{av}^P \approx 0.3 \xi_t^{3/2}, \quad \xi_t \ll 1 \tag{4}$$

$$i_{av}^P = 1 - \frac{1}{\xi_t}, \quad \xi_t > 4. \tag{5}$$

Simulations EM 1 in Table A.2 aimed at verify that the simulators fulfil Eqs. (4)–(5). The top panel in Fig. 4 shows the results of BETsMA, FLEX, and EDTSim for the tape tether. The bottom panel displays the results for BETsMA, EDTSim, and TeMPEST for the round tether. For convenience, we also plotted Eqs. (4)–(5). As shown by the two panels, the match among the simulators and the analytical laws is good. However, there are some differences that should be discussed. First, FLEX does not find numerically the solution of the nonlinear equation that should be solved in the electrical model of Ref. [37]. Instead, the software implements asymptotic solutions of the nonlinear equation [45]. On the other hand, FLEX and BETsMA set equal to zero the current when E_m is negative (i.e., the EE is in the wrong position). However, when E_m is negative, EDTSim and TeMPEST compute the current and voltage profiles by considering a floating tether, i.e., with zero current at the tether tips and considering the electron and ion collection in the anodic and cathodic tether segments. For this reason, the results of these two simulators also exhibit a lower branch of i_{av}. As shown in the inset of the bottom panel in Fig. 4, the agreement among the two software is also good for this lower branch.

In simulations EM 2 in Table A.2, we set $V_C = -50$ V to check for the correct implementation of the EE potential drop. The data from the simulations were filtered to collect particular time steps at which the normalized potential were equal to $\phi_C = -0.60 \pm 0.01$ and $\phi_C = -1.20 \pm 0.01$ for the tape tether (top panel) and to $\phi_C = -0.05 \pm 0.01$ and $\phi_C = -0.20 \pm 0.01$ for the round tether (bottom panel). As expected from Eq. (2), the results lie in a smooth line and the results of the four simulators are consistent, as shown in Fig. 5. A similar conclusion holds from EM 3 (not shown), for which we set $V_C = 0$ and a finite value for the resistance of the resistor.

Previous discussion did not include DYNAT simulations because a separate analysis is needed. Unlike the other simulators that are based on a straight-tether electrical model, DYNAT implements a multiphysics finite element electrical model. It discretizes the tether into several segments and computes the current and voltage profiles by taking into account that, for each element, the projection of the motional electric

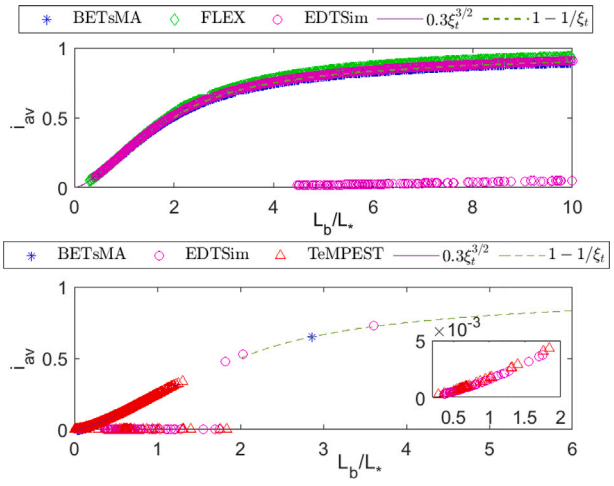

Fig. 4. Normalized average current versus L_b/L_* for simulations EM 1. Top and bottom panels correspond to tape and round tethers.

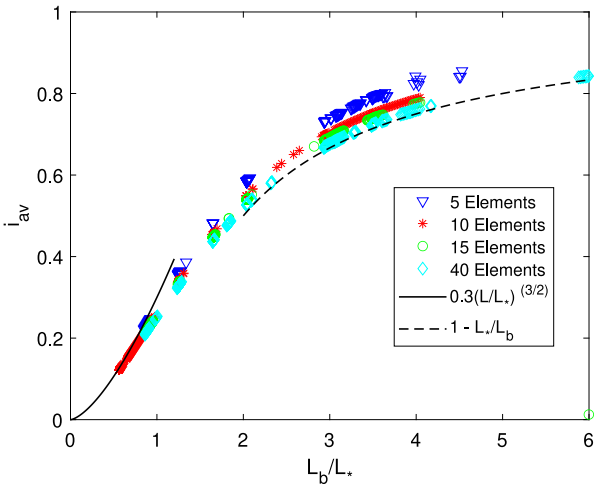

Fig. 6. Normalized average current versus L_b/L_* for simulations EM 1 in DYNAT.

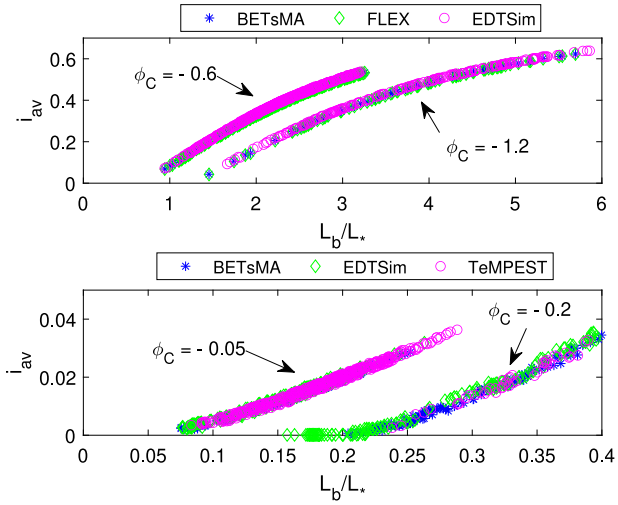

Fig. 5. Normalized average current versus L_b/L_* for simulations EM 2. Top and bottom panels correspond to tape and round tethers.

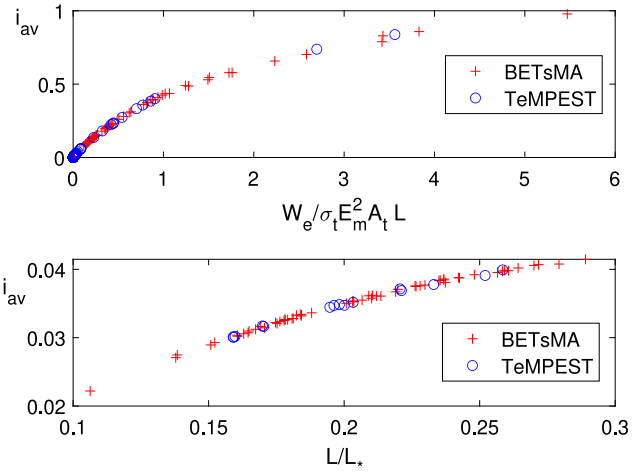

Fig. 7. Top panel: i_{av} versus normalized power for $L_b \approx L_*$ in simulation EM 4. Bottom panel: i_{av} versus L_t/L_* for $W_e/\sigma_t E_m^2 A_t L_t \approx 0.2$ in simulation EM 5.

field along the direction of each segment is different. To cross-check DYNAT, we ran simulation EM 1 and, once finished, filtered the data to select specific instants where the variations of E_m for the elements were smaller than 0.01%. As shown in Fig. 6, it was verified that, for conditions when the tether was almost straight during the simulation, the code predicted Eqs. (4)–(5) for a large enough number of elements. Interestingly, for a low number of elements DYNAT overestimates the tether current.

4.2. The active mode

The standard electrical model for EDTs in the active mode ($E_m < 0$) considers an insulated segment of length L_{ins} between the bare tether of length L_b and a power source that provides a power W_e to drive an electric current in the opposite direction to the motional electric field. For a straight tether, the normalized average current in the active mode (i_{av}^A) depends on the parameter [37,46]

$$i_{av}^A\left(\frac{L_b}{L_*}, \frac{L_{ins}}{L}, \frac{V_C}{|E_m| L_*}, \frac{W_e}{E_m^2 \sigma_t A_t L}\right). \tag{6}$$

In order to cross-verify the electric model in the active mode, we ran simulations EM 4 and EM 5 in Table A.2 with TeMPEST and BETsMA (both of them with a round tether of 2-mm radius). EM 4 involves $V_C = 0$, a long tether of total length equal to 10 km and $L_{ins}/L = 0.4$, and a power input of $W_e = 50$ W. Such a choice is convenient because it allows cross-verification of the simulators with Ref. [46]. The line for $L_b = L_*$ in Fig. 2 of Ref. [46] is in perfect agreement with the top panel of Fig. 7, which corresponds to the simulation results of EM 4 at particular time steps at which the condition $0.96 < L_* < 1.04 L_b$ is met. A second test is shown in the bottom panel of Fig. 7, which presents i_{av} versus L/L_* for EM 5 that considers $V_C = -50$ V, $L = 2$ km, $L_{ins}/L = 0.25$ and $W_e = 50$ W. In order to obtain a smooth line, the results of the simulations were filtered for specific time steps satisfying the conditions $0.197 < W_e/\sigma_t E_m^2 A_t L < 0.203$. This cross-verification of simulations EM 4, EM 5, and the result of Ref. [46], which effectively varied the four dimensionless parameters appearing in Eq. (6), indicate that the electrical model for the tether in the active mode is well implemented in BETsMA and TeMPEST.

5. Tether system performance

After cross-verifying the orbit propagators, the environmental models, and the electric models, it is also possible to make an assessment of the tether system performance provided by the simulators. This is the next logic step because it helps to test the correct implementation of the Lorentz force in the numerical tools. For the analysis, we chose the

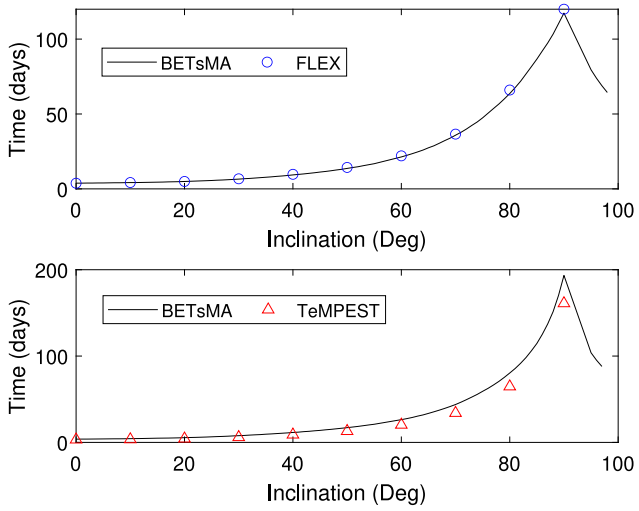

Fig. 8. Deorbit time versus inclination for simulations PER 1 (top) and 2 (bottom).

relationship between the deorbit time and the orbit inclination, which provides an interesting reference scenario with a practical application for EDTs. As shown in Table A.3, we defined two performance simulations: one for tape tethers (PER 1) and the other for round tethers (PER 2). In addition to the parameters given in Table 1 (for tape and round tethers), we used in the simulations the parameters of Table A.3 together with the ones used in simulation EM 1 (see Table 4).

Due to its computational cost, this specific analysis was restricted to the numerical tools that can keep the tether attitude constrained along the local vertical, which are BETsMA, FLEX, and TeMPEST (see right column in Table 4). This decision is also based on intrinsic features of the dynamics of EDTs. A parametric analysis varying the inclination and including tether dynamics, for instance by using a bar-based or a particle-based dynamic model, is very difficult because completing a successful deorbiting maneuver while including tether dynamics needs inevitably the use of passive dampers, an inert tether segment, or the implementation of specific control laws for the current in order to avoid the dynamic instability of EDTs [22]. A detailed design should be done for each inclination and each of the five simulators in this work implement a different strategy to keep the amplitude of the tether oscillations bounded during the deorbit maneuver.

The top panel in Fig. 8 shows the deorbit time versus the orbit inclination for BETsMA and FLEX in PER 1 (tape tether). In this case, the match is almost perfect, as expected by the previous results shown in Sections 3–4. For the case of PER 2 (round tether), the comparison shows that TeMPEST predicts deorbit times slightly shorter than BETsMA. This difference is due to the slightly larger plasma and air densities of TeMPEST (see Section 3).

The performance of the codes is also an interesting topic. Among the relevant figures of merit, the computational cost is probably one of the most important when making decisions about the most suitable code to perform certain analyses on tether systems. However, a quantitative comparison of the computational cost of the five codes is of limited value because, as explained in Section 2, each simulator implements different physical models. Additionally, the simulations were run on different machines. Nonetheless, it is possible to provide an estimation and qualitative information about the computational costs.

Simulations with the tether Aligned along the Local Vertical (ALV) are the ones with the lowest computational cost. They completely ignore tether dynamics and propagate the trajectory of a point mass under the actions of the Lorentz force and the other perturbation forces. As shown in the right column of Table 4, BETsMA, DYNAT, FLEX, and TeMPEST can do simulations with the ALV model. To give a reference point for the computational cost, we mention that BETsMA in the ALV mode and using a fixed time-step Runge–Kutta integrator can simulate about 0.6 days of mission per second by using a laptop (3.2-GHz CPU). The computational cost increases considerably when tether dynamics is included in the simulations and it depends strongly on the type of tether model. For instance, if the tether is modelled as a set of rigid bars (inelastic-but-flexible tether model), the short scale of the fast longitudinal waves along the tether are removed and some computational resources can be saved. For BETsMA, and using two rigid bars for modelling the tether, the computational cost using an implicit and variable-time-step Radau integrator is about 0.8 days per hour (2.1-GHz CPU). The most demanding simulations are the ones with elastic tethers, which can be modelled as a set of lumped masses (LM) or a continuous tether model (a partial differential equation). BETsMA, EDTSim, and FLEX do implement the former. To give a reference, the computational cost of an EDTSim simulation using 41 mass points is about 2.4 days of simulation per day using a 3.40-GHz CPU. In the case of the continuous tether model of DYNAT, the computational cost is about 1.2 days of simulation per day using 10 tether elements and a 4.2-GHz CPU.

6. Conclusions

This work cross-verified the key components of five EDT simulators: BETsMA, DYNAT, FLEX, EDTSim, and TeMPEST. These key components include their orbit propagators, environmental models, electrical model in the passive mode, and overall performance of an EDT system (deorbit time versus inclination). Although each code has a different architecture and may use different environmental models, orbit propagator, numerical integrator, etc., a good agreement has been found among them. Therefore, the results indicate that the simulation data that have been published in a public repository as part of this work is relevant information to boost the development of tether software.

During the process of cross-verifying the five simulators, we found some implementation errors in some of the software that, although they would not have affected the overall conclusion about previous mission analysis and/or performance assessment, it is important to eliminate. Such flaws have been only detected after making the comparison presented in this work and thanks to the reference cases that have been created. Their identification from the results of a single code was difficult due to the high complexity of EDT simulators. This experience suggests that the repository of data generated in this work may be useful for the tether community.

In addition to the simulation results, tables summarizing the capabilities and the physical and numerical models implemented by the five simulators have been prepared. They provide a broad view of the state-of-the-art of EDT simulators. Quantitative values of the computational cost have also been provided and related to the degree of fidelity of the models. As expected, the cost is mainly driven by the type of tether dynamic model (aligned with the local vertical or spinning at a prescribed angular velocity, flexible and inelastic, or flexible and elastic). Therefore, the information provided in this work is relevant to make an informed decision on the best software to carry out a given analysis.

The work intentionally omitted certain modules of EDT simulators that are beyond the scope of this study. The most important is the module responsible for simulating tether dynamics. As shown in Table 4, flexible and inelastic N-bar models, flexible and elastic lumped mass models, and continuous models are available in some of the simulators discussed in this work. They may be cross-verified in a future work to complement the database of public simulations.

Declaration of competing interest

The authors declare that they have no known competing financial interests or personal relationships that could have appeared to influence the work reported in this paper.

Acknowledgements

This work was supported by the European Union's Horizon 2020 Research and Innovation Programme (No 828902, E.T.PACK project) and by Natural Sciences and Engineering Research Council of Canada, Discovery Grant (RGPIN-2018-05991). TeMPEST development was supported by NASA's Tethered Satellite System mission office via support to the Shuttle Electrodynamic Tether System (NASA contract NAS8-93831; lead software developer: N. Voronka).

Appendix. List of simulations

See Tables A.1–A.3

Table A.1
Simulations aimed at the verification of the Orbit Propagators and the Environmental (OPE) models. All the simulations have initial conditions with zero argument of the perigee, right ascension, and true anomaly. Simulation start time is 00:00:00 of January 1st, 2000.

Code	Initial orbit	Perturbations
OPE 1	$e = 0.005$, $i = 0°$	None
OPE 2	$e = 0.005$, $i = 90°$	None
OPE 3	$e = 0.000$, $i = 0°$	J2
OPE 4	$e = 0.000$, $i = 75°$	J2
OPE 5	$e = 0.000$, $i = 90°$	J2
OPE 6	$e = 0.000$, $i = 98°$	J2
OPE 7	$e = 0.005$, $i = 0°$	J2
OPE 8	$e = 0.005$, $i = 90°$	J2
OPE 9	$e = 0.000$, $i = 75°$	SH (4th)
OPE 10	$e = 0.005$, $i = 98°$	SH (4th)

Table A.2
Summary of the simulations to verify the electrical models. All the initial conditions have vanishing argument of the perigee, right ascension, and true anomaly, and $e = 0.005$, inc $= 60°$, $H_0 = 600$ km. Simulation start time is 00:00:00 of January 1st, 2000.

Code	Mode	Parameters
EM 1	Passive	$L_b = 2$ km, $V_c = 0$ V, $R = 0$ Ω, $W_e = 0$ W
EM 2	Passive	$L_b = 2$ km, $V_c = -50$ V, $R = 0$ Ω, $W_e = 0$ W
EM 3	Passive	$L_b = 2$ km, $V_c = 0$ V, $R = 50$ Ω, $W_e = 0$ W
EM 4	Active	$L_b = 6$ km, $V_c = 0$ V, $L_{ins} = 4$ km, $W_e = 50$ W
EM 5	Active	$L_b = 1.5$ km, $V_c = -50$ V, $L_{ins} = 500$ m, $W_e = 50$ W

Table A.3
Simulations aimed at the verification of performances of EDTs. All the simulations have initial conditions with zero argument of the perigee, right ascension, and true anomaly. Simulation start time is 00:00:00 of January 1st, 2000.

Code	Parameters
PER 1	Tape tether (2 km × 2 cm × 50 μm) + EM 1
PER 2	Round tether (2 km × 2 mm) + EM 1

References

[1] S.D. Drell, H.M. Foley, M.A. Ruderman, Drag and propulsion of large satellites in the ionosphere: An Alfvén propulsion engine in space, J. Geophys. Res. 70 (13) (1965) 3131–3145, http://dx.doi.org/10.1029/JZ070i013p03131.

[2] J.R. Sanmartin, E.C. Lorenzini, Martinez-Sanchez, Electrodynamic tether applications and constraints, J. Spacecr. Rockets 47 (2010) 442–456, http://dx.doi.org/10.2514/1.45352.

[3] M.D. Grossi, Plasma Motor Generator (PMG) Electrodynamic Tether Experiment, Final Report of NASA Grant NAG9-643 June, Smithsonian Institute Astrophysical Observatory, Cambridge Massachusetts, 1995, pp. 1–4.

[4] N.P. Singh, W.C. Leung, Numerical simulation of plasma processes occurring in the RAM region of the tethered satellite, Geophys. Res. Lett. 25 (1998) 741–744.

[5] S. Bilén, B. Gilchrist, Transient plasma sheath model for thin conductors excited by negative high voltages with application to electrodynamic tethers, IEEE Trans. Plasma Sci. 28 (6) (2000) 2058–2074, http://dx.doi.org/10.1109/27.902233.

[6] T. Onishi, M. Martinez-Sanchez, D.L. Cooke, Computation of a moving bare tether, AIP Conf. Proc. 552 (1) (2001) 488–493, http://dx.doi.org/10.1063/1.1357966.

[7] J.A. Janeski, W.A. Scales, C.D. Hall, Investigation of the current collected by a positively biased satellite with application to electrodynamic tethers, J. Geophys. Res. (Space Phys.) 119 (9) (2014) 7824–7840, http://dx.doi.org/10.1002/2013JA019473.

[8] P. Janhunen, Boltzmann electron PIC simulation of the E-sail effect, Ann. Geophys. 33 (12) (2015) 1507–1512, http://dx.doi.org/10.5194/angeo-33-1507-2015, URL https://angeo.copernicus.org/articles/33/1507/2015/.

[9] G. Xia, Y. Han, L. Chen, Y. Wei, Y. Yu, M. Chen, Simulations of momentum transfer process between solar wind plasma and bias voltage tethers of electric sail thruster, Acta Astronaut. 147 (2018) 107–113, http://dx.doi.org/10.1016/j.actaastro.2018.03.049.

[10] R. Marchand, G.L. Delzanno, Tethered capacitor charge mitigation in electron beam experiments, Front. Astron. Space Sci. 5 (2018) 42, http://dx.doi.org/10.3389/fspas.2018.00042.

[11] R. Choinière, B.E. Gilchrist, Self-consistent 2-D kinetic simulations of high-voltage plasma sheaths surrounding ion-attracting conductive cylinders in flowing plasmas, IEEE Trans. Plasma Sci. 35 (2007) 7–22, http://dx.doi.org/10.1109/TPS.2006.889300.

[12] X. Chen, G. Sanchez-Arriaga, Orbital motion theory and operational regimes for cylindrical emissive probes, Phys. Plasmas 24 (2) (2017) 023504, http://dx.doi.org/10.1063/1.4975088.

[13] L. Chiabó, S. Shahsavani, G. Sánchez-Arriaga, Kinetic analysis of the plasma sheath around an electron-emitting object with elliptic cross section, Phys. Rev. E 104 (2021) 055204, http://dx.doi.org/10.1103/PhysRevE.104.055204, URL https://link.aps.org/doi/10.1103/PhysRevE.104.055204.

[14] G. Sánchez-Arriaga, D. Pastor-Moreno, Direct Vlasov simulations of electron-attracting cylindrical Langmuir probes in flowing plasmas, Phys. Plasmas 21 (2014) 073504.

[15] R. Hoyt, Design and simulation of a tether boost facility for LEO to GTO transport, in: 36th AIAA/ASME/SAE/ASEE Joint Propulsion Conference and Exhibit, 2000, http://dx.doi.org/10.2514/6.2000-3866, arXiv:https://arc.aiaa.org/doi/pdf/10.2514/6.2000-3866, URL https://arc.aiaa.org/doi/abs/10.2514/6.2000-3866.

[16] S. Bilén, J. McTernan, B. Gilchrist, I. Bell, N. Voronka, R. Hoyt, Electrodynamic tethers for energy harvesting and propulsion on space platforms, in: AIAA SPACE 2010 Conference & Exposition, American Institute of Aeronautics and Astronautics, 2010, http://dx.doi.org/10.2514/6.2010-8844.

[17] R. Mantellato, L. Olivieri, E. Lorenzini, Study of dynamical stability of tethered systems during space tug maneuvers, Acta Astronaut. 138 (2017) 559–569, http://dx.doi.org/10.1016/j.actaastro.2016.12.011.

[18] G. Li, Z.H. Zhu, Multiphysics finite element modeling of current generation of bare flexible electrodynamic tether, J. Propuls. Power 33 (2) (2017) 408–419, http://dx.doi.org/10.2514/1.B36211.

[19] G. Sánchez-Arriaga, C. Bombardelli, X. Chen, Impact of nonideal effects on bare electrodynamic tether performance, J. Propuls. Power 31 (3) (2015) 951–955, http://dx.doi.org/10.2514/1.B35393.

[20] G. Sánchez-Arriaga, G. Borderes-Motta, L. Chiabó, A code for the analysis of missions with electrodynamic tethers, Acta Astronaut. 198 (2022) 471–481, http://dx.doi.org/10.1016/j.actaastro.2022.06.021.

[21] S. Kawamoto, Y. Ohkawa, T. Okumura, K. Iki, H. Okamoto, Performance of electrodynamic tether system for debris deorbiting: Re-evaluation based on the results of KITE experiments, in: 69th International Astronautical Congress, IAC, Bremen, Germany, IAC-18- A6.6.5, 2018, pp. 1–5.

[22] J. Pelaez, E.C. Lorenzini, O. Lopez-Rebollal, M. Ruiz, A new kind of dynamic instability in electrodynamic tethers, in: Advances in the Astronautical Sciences, Vol. 105, 1367–1386, Spaceflight Mechanics, AAS Publications, San Diego, CA, 2000., P.1367, Vol. 105, 2000, pp. 1367–1386.

[23] E.L.M. Lanoix, A.K. Misra, V.J. Modi, G. Tyc, Effect of electromagnetic forces on the orbital dynamics of tethered satellites, J. Guid. Control Dyn. 28 (6) (2005) 1309–1315, http://dx.doi.org/10.2514/1.1759.

[24] E.M. Levin, J. Pearson, J.C. Oldson, Dynamics Simulation Model for Space Tethers, NASA/CR—2006–214432, 2006, pp. 1–70, http://dx.doi.org/10.1016/S0045-7825(01)00163-3, Available from NASA Center for AeroSpace Information.

[25] J.R. Ellis, C.D. Hall, Model development and code verification for simulation of electrodynamic tether system, J. Guid. Control Dyn. 32 (6) (2009) 1713–1722, http://dx.doi.org/10.2514/1.44638.

[26] K. Kristiansen, P. Palmer, R. Roberts, Numerical modelling of elastic space tethers, Celestial Mech. Dynam. Astronom. 113 (2012) http://dx.doi.org/10.1007/s10569-012-9411-5.

[27] R. Zhong, Z.H. Zhu, Dynamics of nanosatellite deorbit by bare electrodynamic tether in low Earth orbit, J. Spacecr. Rockets 50 (3) (2013) 691–700, http://dx.doi.org/10.2514/1.A32336.

[28] C. Bombardelli, D. Zanutto, E. Lorenzini, Deorbiting performance of bare electrodynamic tethers in inclined orbits, J. Guid. Control Dyn. 36 (5) (2013) 1550–1556, http://dx.doi.org/10.2514/1.58428.

[29] H. Wen, D. Jin, H. Hu, Three-dimensional deployment of electro-dynamic tether via tension and current control with constraints, Acta Astronaut. 129 (2016) 253–259, http://dx.doi.org/10.1016/j.actaastro.2016.09.019, URL http://www.sciencedirect.com/science/article/pii/S0094576516306099.

[30] K. Xie, H. Yuan, F. Liang, W. Wang, Q. Xia, Lorentz force characteristics of a bare electrodynamic tether system with a hollow cathode, J. Astronaut. Sci. 68 (2021) 327–348, http://dx.doi.org/10.1007/s40295-021-00256-1.
[31] V.V. Beletsky, E.M. Levin, Dynamics of Space Tether Systems, American Astronautical Society, 1993.
[32] E.M. Levin, Dynamic Analysis of Space Tether Missions, American Astronautical Society, 2007.
[33] V. Aslanov, A.S. Ledkov, Dynamics of Tethered Satellite Systems, Woodhead Publishing, 2012.
[34] H. Troger, A. Alpatov, V. Beletsky, V. Dranovskii, V. Khoroshilov, A. Pirozhenko, A. Zakrzhevskii, Dynamics of Tethered Satellite Systems, CRC Press, 2017.
[35] A. Minakov, Fundamentals of the Thread Mechanics, Moscow Textile Institute, 1941.
[36] P.T. Williams, A review of space tether technology, 2012, pp. 22–36, Recent Patents on Space Technology, 2.
[37] J.R. Sanmartin, M. Martinez-Sanchez, E. Ahedo, Bare wire anodes for electrodynamic tethers, J. Propul. Power 9 (1993) 353–360, http://dx.doi.org/10.2514/3.23629.
[38] X. Chen, J.R. Sanmartín, Low work-function thermionic emission and orbital-motion-limited ion collection at bare-tether cathodic contact, Phys. Plasmas 22 (5) (2015) http://dx.doi.org/10.1063/1.4919945, URL http://scitation.aip.org/content/aip/journal/pop/22/5/10.1063/1.4919945.
[39] G. Sánchez-Arriaga, J.R. Sanmartín, Electrical model and optimal design scheme for low work-function tethers in thrust mode, Aerosp. Sci. Technol. 96 (2020) 105519.
[40] G. Borderes-Motta, G.d. Haro-Pizarroso, G. Li, H. Yu, Z. H. Zhu, G. Sarego, G. Colombatti, E.C. Lorenzini, J.K. McTernan, B.E. Gilchrist, S.G. Bilén, S. Kawamoto, Y. Ohkawa, G. Sanchez-Arriaga, Dataset of the Cross-Verification and Benchmarking Analysis of Electrodynamic Tether Simulators, e-cienciaDatos, 2022, http://dx.doi.org/10.21950/FL2DG6.
[41] J. Peláez, J.M. Hedo, P.R. de Andrés, A special perturbation method in orbital dynamics, Celestial Mech. Dynam. Astronom. 97 (2) (2007) 131–150, http://dx.doi.org/10.1007/s10569-006-9056-3.
[42] G. Sánchez-Arriaga, X. Chen, Modeling and performance of electrodynamic low-work-function tethers with photoemission effects, J. Propuls. Power 34 (1) (2018) 213–220, http://dx.doi.org/10.2514/1.B36561.
[43] M. Tajmar, G. Sánchez-Arriaga, A bare-photovoltaic tether for consumable-less and autonomous space propulsion and power generation, Acta Astronaut. 180 (2021) 350–360, http://dx.doi.org/10.1016/j.actaastro.2020.12.053, URL https://www.sciencedirect.com/science/article/pii/S0094576520307967.
[44] E. Ahedo, J.R. Sanmartín, Analysis of bare-tether systems for deorbiting low-earth-orbit satellites, J. Spacecr. Rockets 39 (2002) 198–205, http://dx.doi.org/10.2514/2.3820.
[45] C. Bombardelli, J. Pelaez, M. Sanjurjo, Asymptotic solution for the current profile of passive bare electrodynamic tethers, J. Propuls. Power 26 (6) (2010) 1291–1304, http://dx.doi.org/10.2514/1.46808.
[46] J.R. Sanmartin, R.D. Estes, E.C. Lorenzini, S.A. Elaskar, Efficiency of electrodynamic tether thrusters, J. Spacecr. Rockets 43 (3) (2006) 659–666, http://dx.doi.org/10.2514/1.16174.